2021 43rd Annual International Conference of the
IEEE Engineering in Medicine & Biology Society (EMBC)
Oct 31 - Nov 4, 2021. Virtual Conference

A Multiscale Model to Identify Limiting Factors in Nanoparticle-Based miRNA Delivery for Tumor Inhibition*

Prashant Dogra, Javier Ruiz Ramírez, Joseph D. Butner, Maria J. Peláez, Vittorio Cristini, and Zhihui Wang, *Member, IEEE*

***Abstract*—MicroRNA-based gene therapy for cancer treatment via nanoparticles (NPs) requires navigation of multiple physical and physiological barriers in order to efficiently deliver the miRNAs to the cancer cell cytoplasm. We here present a mathematical model to investigate the variability associated with tumor, NP, and miRNA characteristics, and identify the limiting factors in miRNA delivery to tumors. Through global parameter analysis, the miRNA release rate from NPs and NP degradability were found to have the most significant impact on cytosolic accumulation of miRNAs. These NP properties can be fine-tuned in order to optimize the delivery system for enhancing the efficacy of miRNA-based therapy.**

***Clinical Relevance*—Understanding the effect of nanoparticle, tumor, and miRNA characteristics in governing the efficacy of miRNA-based cancer therapy will support its clinical translation.**

I. Introduction

MicroRNAs (miRNAs) are small non-protein-coding RNAs (~22 nucleotides) that regulate cell signaling by binding to genes that code for proteins, thereby inhibiting protein translation. It is increasingly recognized that miRNA dysregulation causes aberrant cell signaling associated with cancer. miRNAs are either found to be downregulated [1] or upregulated [2] in tumors, which manifests as downregulation of tumor suppressor effects and upregulation of oncogenic effects, respectively. Therefore, exogenous administration of miRNAs or their antagonists to normalize aberrant signaling pathways is currently an attractive approach to inhibit tumor cell proliferation. However, given the short half-life of naked miRNAs due to degradation by plasma ribonucleases, limited tumor penetration and cellular uptake due to their negative charges, and off-target effects due to non-specific delivery, nanoparticle (NP)-based delivery systems have been used to ensure targeted and efficient delivery to tumor cells [3]. Whereas the application of nanomaterials in cancer has shown potential to improve targeted drug delivery to tumors [4, 5], challenges with low tumor deliverability due to insufficient understanding of the collective effects of NP properties on NP pharmacokinetics and tumor penetration still exist. To this end, mechanistic mathematical modeling can be used as a valuable in-silico tool [6-8] to improve the understanding of NP-mediated miRNA delivery to cancer cells *in vivo*, and can provide practical guidelines to optimize NP design for enhanced miRNA therapy efficacy.

*The work was supported in part by the National Science Foundation grant DMS-1930583 (V.C., Z.W.), National Institutes of Health grants 1R01CA253865 (V.C., Z.W.), 1U01CA196403 (V.C., Z.W.), 1U01CA213759 (V.C., Z.W.), 1R01CA226537 (V.C., Z.W.), 1R01CA222007 (V.C., Z.W.) and U54CA210181 (V.C., Z.W.).

II. Methods

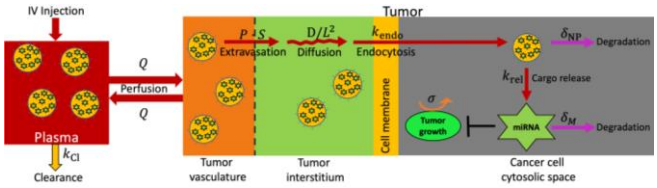

Figure 1. Model schematic. Model consists of a plasma and tumor compartment, with the latter sub-compartmentalized into vascular, interstitial, cell membrane, and cell cytosolic space. Yellow circles represent nanoparticles (NPs) loaded with miRNAs (green stars). Red arrows indicate transport processes. Curved orange arrow indicates tumor growth. Black hammerhead indicates inhibition of tumor proliferation. Magenta arrows represent degradation and yellow arrow indicates clearance of NPs.

A. Model development

We have developed a multiscale mechanistic model, calibrated to mice, to study the pharmacokinetics and pharmacodynamics of NP-delivered, miRNA-based cancer therapy. As shown in Fig. 1, the model consists of a plasma (systemic circulation) and a tumor compartment, where the latter is further divided into vasculature, interstitium, and cytosolic sub-compartments. Following intravenous (i.v.) injection of miRNA-loaded NPs into the plasma compartment, NPs are cleared from the systemic circulation via renal and/or hepatobiliary excretion mechanisms (based on their physicochemical characteristics) [9, 10]. In the current model, clearance is parameterized by k_{Cl} (units, wk^{-1}), which empirically varies with NP diameter (ϕ_{NP}; units, cm) as: $k_{\mathrm{Cl}} = \frac{\ln(2)}{0.11\cdot e^{-1.33\cdot\phi_{\mathrm{NP}}} - 0.001\cdot e^{-9.7\cdot\phi_{\mathrm{NP}}}}$, obtained by fitting the plasma half-life data of quantum dots of varying sizes from the literature [10, 11].

NPs circulating in the plasma compartment are transported between the plasma and tumor vasculature sub-compartment via perfusion, defined by the plasma flow rate Q (units, $\mathrm{mL}\cdot g^{-1}\cdot\mathrm{wk}^{-1}$), which is determined by the following empirical relationship with tumor volume $B(t)$ (units, cm^3): $Q = 2843\cdot e^{-0.65\cdot B(t)}$, obtained by fitting a monoexponential function to data reported in [12]. From the tumor vascular sub-compartment, NPs can unidirectionally permeate and accumulate in the tumor extravascular regions to deliver the cargo to the cancer cells (a phenomenon referred to as the enhanced permeability and retention (EPR) effect). As shown in Fig. 1, we model this serial process in three steps, characterized by the following rate constants. *i)* The

P.D., J.R.R., J.D.B., M.J.P., V.C., and Z.W. are with the Mathematics in Medicine Program, Houston Methodist Research Institute, Houston, TX 77030, USA. V.C. and Z.W. are also with Weill Cornell Medicine. V.C. is also with Department of Imaging Physics, University of Texas MD Anderson Cancer Center, Houston, TX 77230, USA (corresponding author, e-mail: zwang@houstonmethodist.org).

extravasation rate of NPs from the vascular to interstitial sub-compartment is characterized by the permeability (P)-surface area (S) product ($P \cdot S$), where P (units, $\text{cm} \cdot \text{wk}^{-1}$) is a function of tumor vascular porosity and the ratio of NP size (ϕ_{NP}) to tumor vascular pore size (ϕ_{pore}; units, cm) [13], and S (units, cm^2/cm^3) relates to tumor volume $B(t)$ as $S = 0.26 \cdot e^{-4.5 \cdot B(t)} + 138 \cdot e^{-0.04 \cdot B(t)}$, obtained empirically from data in the literature [14]. *ii)* The diffusion rate of NPs across the tumor interstitium to reach the cancer cells is characterized by the ratio D/L^2, where D is NP diffusivity (units, $\text{cm}^2 \cdot \text{wk}^{-1}$) and L is the intercapillary distance (units, cm), suggestive of the characteristic length of the interstitium between tumor vessels and cancer cells. *iii)* Once in the vicinity of cancer cells, NPs undergo endocytosis (characterized by the rate of endocytosis (k_{endo}; units, wk^{-1})) to enter the cell cytosolic region.

The endocytosed NPs then release miRNAs into the cytoplasm at a rate characterized by k_{rel} (units, wk^{-1}), while undergoing degradation inside the endosome at a rate δ_{NP} (units, wk^{-1}). The released miRNAs act on their target site (messenger RNA molecules) to suppress protein translation and exhibit tumor suppressor effects, so the tumor growth rate constant σ (units, wk^{-1}) is scaled by the dimensionless factor $1/(1 + \frac{C_M(t)}{\text{EC}_{50}})$, where $C_M(t)$ is the cytosolic concentration of miRNA and EC_{50} is the concentration of miRNA inducing half of the maximum possible tumor inhibition. Inside the cytosol, miRNA also undergoes degradation characterized by the rate constant δ_{M} (units, wk^{-1}). The various model parameters were either known a priori or obtained through data fitting from the literature (Table I).

TABLE I. LIST OF MODEL PARAMETERS STUDIED IN GSA

Notation	Description	Units	Value (Range)[a]	Ref.
Tumor-associated parameters				
σ	Tumor growth rate constant	wk^{-1}	2.99 (1.3-6.5)	[15]
ϕ_{pore}	Dia. of tumor vessel pore	nm	1700 (300-4700)	[16]
L	Tumor intercapillary length	μm	100 (10-250)	[17]
$\eta_{T,B}$	Dynamic viscosity of tumor blood	cP	7.42 (4.5-10)	[14]
$\eta_{T,I}$	Dynamic viscosity of tumor interstitium	cP	3.5 (2-5)	[18]
NP-associated parameters				
ϕ_{NP}	Dia. of NP	nm	70 (25-150)	–
δ_{NP}	NP degradation rate	wk^{-1}	0.1 (0.01-1)	arb.
N_0	No. of NPs per injection (represents dose of miRNA)	–	2.5e+10 (6.4e+9 - 1e+12) ≡ 4μg miRNA (1-156 μg)	calc.
miRNA-associated parameters				
EC_{50}	EC_{50} of miRNA	nM	1 (0.1-100)	[19]
k_{rel}	Release rate of miRNA from NPs	wk^{-1}	0.42 (0.16-9.7)	arb.
δ_M	Decay rate of miRNA	wk^{-1}	4.8 (2.4-29.1)	[20]

[a]Parameter value range used for GSA

B. Model equations

The various transport and pharmacodynamic processes described above have been formulated into a system of ordinary differential equations (ODEs; Eqs. 1–7) to numerically simulate a reference treatment protocol. We then used the model to further understand the role of different model parameters in governing NP and miRNA delivery, and treatment outcome.

Equation for NP mass kinetics in plasma ($N_P(t)$):

$$\frac{dN_P(t)}{dt} = \left(\frac{N_V(t)}{V_{T,V}} - \frac{N_P(t)}{V_P}\right) \cdot Q \cdot B(t) - k_{\text{Cl}} \cdot N_P(t), \quad N_P(t) = \begin{cases} 0, t = 0 \\ N_0, t = i \end{cases} \quad (1)$$

where, $V_{T,V}$ ($= f_v * B(t)$) and V_P (1 mL) [21] are volumes of tumor vascular and plasma compartments, respectively; f_v ($= 0.17$) is the vascular fraction of the tumor [14]; N_0 is the injected dose of NPs and i represents the injection times (in weeks) post inoculation of tumor in mice ($i = 2, 3, 4, 5$).

Equation for NP mass kinetics in tumor vasculature ($N_V(t)$):

$$\frac{dN_V(t)}{dt} = \left(\frac{N_P(t)}{V_P} - \frac{N_V(t)}{V_{T,V}}\right) \cdot Q \cdot B(t) - P \cdot S \cdot N_V(t), \quad N_V(0) = 0 \quad (2)$$

Equation for NP mass kinetics in tumor interstitium ($N_I(t)$):

$$\frac{dN_I(t)}{dt} = P \cdot S \cdot N_V(t) - \frac{D}{L^2} \cdot N_I(t), \qquad N_I(0) = 0 \quad (3)$$

Equation for NP mass kinetics in cancer cell membrane ($N_M(t)$):

$$\frac{dN_M(t)}{dt} = \frac{D}{L^2} \cdot N_I(t) - k_{\text{endo}} \cdot N_M(t), \qquad N_M(0) = 0 \quad (4)$$

Equation for NP mass kinetics in cancer cell cytosol ($N_C(t)$):

$$\frac{dN_C(t)}{dt} = k_{\text{endo}} \cdot N_M(t) - \delta_{\text{NP}} \cdot N_C(t), \qquad N_C(0) = 0 \quad (5)$$

Equation for miRNA concentration kinetics in cancer cell cytosol ($C_M(t)$):

$$\frac{dC_M(t)}{dt} = k_{\text{rel}} \cdot \frac{N_C(t) \cdot M_0 \cdot e^{-k_{\text{rel}} \cdot t}}{V_{T,C}} - \delta_M \cdot C_M(t), \quad C_M(0) = 0 \quad (6)$$

where M_0 is the mass of miRNAs loaded in a single NP; $V_{T,C}$ is the cytosolic volume of tumor ($= f_c * f_{\text{cy}} * B(t)$), where f_c ($= 0.4$) is the cancer cell volume fraction of a tumor [22] and f_{cy} ($= 0.4$) is the cytoplasmic volume fraction of a cancer cell [23]. Note that the concentration of tumor suppressive miRNAs is downregulated in cancer; therefore, it is reasonable to assume its initial condition to be zero.

Equation for tumor volume kinetics ($B(t)$):

$$\frac{dB(t)}{dt} = \frac{\sigma}{1 + \frac{C_M(t)}{\text{EC}_{50}}} \cdot \left(1 - \frac{B(t)}{B^*}\right) \cdot B(t), \qquad B(0) = B_0 \quad (7)$$

where B_0 is the inoculated size of tumor (0.001 cm^3 = 10^6 cells) [24] and B^* is the tumor carrying capacity (1 cm^3).

The model is solved numerically as an initial value problem in MATLAB R2018a using the built-in function *ode45*.

C. Parametric and statistical analyses

To understand the effect of various delivery barriers, and physicochemical and physiological processes on NP-mediated miRNA delivery to the tumor cytosolic space, which in turn affects tumor inhibition, we performed global

sensitivity analysis (GSA). In our analysis, a total of 11 model parameters were simultaneously perturbed from their baseline value (within a predefined physiological range, Table I). We focused on the following six model outputs of interest: $\mathrm{AUC}_{P}^{\mathrm{NP}}$, $\mathrm{AUC}_{T,V}^{\mathrm{NP}}$, $\mathrm{AUC}_{T,I}^{\mathrm{NP}}$, $\mathrm{AUC}_{T,C}^{\mathrm{NP}}$, $\mathrm{AUC}_{T,C}^{M}$, and t_{90}, which represent area under the curve (AUC) of NP mass kinetics in -plasma, -tumor vasculature, -tumor interstitium, -tumor cytosol, miRNA concentration kinetics in tumor cytosol, and time to reach 90% of carrying capacity, respectively. While AUCs are indicative of bioavailability of NPs or miRNA in a given compartment, t_{90} indicates inhibition of tumor proliferation. Note that AUC is calculated through numerical integration using the built-in MATLAB function *trapz*. To investigate the vast multidimensional parameter space, Latin hypercube sampling was used to obtain 11,000 sets of parameters, ten times. Each of the ten parameter batches and their corresponding model outputs was subject to multivariate linear regression analysis to obtain a distribution of regression coefficients for each parameter, which served as the sensitivity index (SI) to quantify the significance of the parameters in governing the model outputs. Finally, one-way ANOVA and Tukey's test were conducted to rank the parameters in order of their SI value (higher the SI, the more sensitive the measured output is to changes in the parameter) [25-28]. All analyses were performed in MATLAB R2018a.

III. Results and Discussion

Treatment simulation and global sensitivity analysis

We used the model to simulate a literature-based treatment regimen of miRNA therapy [24], which involves a weekly IV injection of 0.15 mg·kg^{-1} miRNA (equivalent to 4 μg/mouse of miRNA) for 4 weeks, starting 2 weeks post tumor inoculation. Of note, the number of NPs (reference size: 70 nm in diameter) required to load the reference dose of 4 μg miRNA is ~2.5e+10; this number was estimated based on NP volume, molecular weight of miRNA (~7kDa [29]), and the assumptions that the miRNA is a sphere of dia. ~2.5 nm [30] and packed randomly into a hollow NP with a packing efficiency of ~64% [31]. In our GSA, to simulate a different NP size (or miRNA dose) other than the reference value, we had to recalculate the number of NPs required to load a given dose. Also, to be consistent with other reports in the field, NP mass was represented by percent of injected dose (%ID), instead of actual number of NPs in a given compartment.

As shown in Fig. 2, the numerical solution of the model, based on the reference parameter values (Table I and Methods) and the implemented treatment regimen, appropriately predicted the temporal evolution of NP mass in various model compartments (Fig. 2a-2d), miRNA concentration in cancer cell cytosol (Fig. 2e), and tumor size (Fig. 2f). Following each injection, NP kinetics in the plasma was primarily governed by clearance mechanisms, represented by the lumped k_{Cl} parameter, leading to almost complete elimination of the injected dose within a week (Fig. 2a). Further substantiated by GSA (Fig. 3a), NP size (ϕ_{NP}), which exerts its impact by modulating k_{Cl}, was found to be the most significant parameter in affecting NP bioavailability in plasma ($\mathrm{AUC}_{P}^{\mathrm{NP}}$).

From the systemic circulation, the blood flow-dependent delivery to tumor causes an incremental change in NP mass in

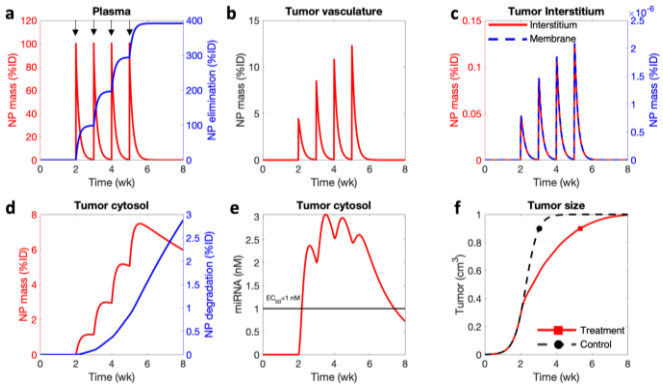

Figure 2. Treatment simulation. Model predicted kinetics of NP mass (% injected dose (%ID)) in **a**) –plasma (left y-axis), **b**) –tumor vasculature, **c**) – tumor interstitium (left y-axis), –cancer cell membrane (right y-axis), **d**) – tumor cytosol (left y-axis), **e**) miRNA concentration in tumor cytosol, and **f**) tumor volume is shown. Note: right y-axis in panel **a**) corresponds to NP elimination kinetics from plasma; black arrows on top of panel **a**) indicate the injection time-points; right y-axis in panel **d**) represents NP degradation kinetics in tumor cytosol; black line in panel **e**) indicates the reference EC_{50} value of miRNA; and markers in panel **f**) indicate 90% of carrying capacity, such that the corresponding abscissas are the t_{90} values.

tumor vasculature with every injection (Fig. 2b), which is attributable to incremental rise of NP mass with every injection in plasma compartment (Fig. 2a), due to the remaining residual of the previous injection (change conspicuous in logscale, not shown). Additionally, as shown in Fig. 3b, tumor growth rate constant σ is the most significant parameter in affecting NP bioavailability in tumor vasculature ($\mathrm{AUC}_{T,V}^{\mathrm{NP}}$), which suggests that due to the growing tumor the rate of influx of NPs into the tumor vasculature increases with time because the tumor vasculature volume increases in parallel with the tumor volume (first term of Eq. 2), thereby causing the increments.

Further, NP mass kinetics in the tumor interstitium is coupled to tumor vascular kinetics (Fig. 2c), suggesting that permeation into or diffusion through the interstitium is not a rate limiting factor for the given baseline conditions of NP and tumor characteristics. However, as we identified through GSA (Fig.3c), L, $\eta_{T,B}$ (tumor blood viscosity), $\eta_{T,I}$, and ϕ_{pore} (tumor vessel wall pore size) are significant in affecting the NP bioavailability in tumor interstitium ($\mathrm{AUC}_{T,I}^{\mathrm{NP}}$), which suggests that under a different set of parameter values (e.g., a hypovascular, or densely stromal, or tumor with smaller vessel wall pores, or larger NPs), we may observe decoupling from vascular kinetics that can make extravasation or interstitial diffusion a limiting factor in delivery to the cytosol.

Similarly, endocytosis through the membrane, which is a relatively fast process depending upon NP size (ϕ_{NP}), does not decouple from vascular kinetics in limiting delivery to the inside of the cell for the studied NP size (Fig. 2c). However, as shown in Fig. 3d, ϕ_{NP} is one of the most significant factors that affect the NP bioavailability in tumor cytosol ($\mathrm{AUC}_{T,C}^{\mathrm{NP}}$), in addition to the degradation rate of the NP (δ_{NP}), suggesting that cytosolic accumulation of NPs is sensitive to their size and degradability. Moreover, as shown in Fig. 2d, the characteristics of the hypothetical NPs used in the simulations allow incremental accumulation of NPs in the cytosol with every injection, eventually surpassing the well-accepted

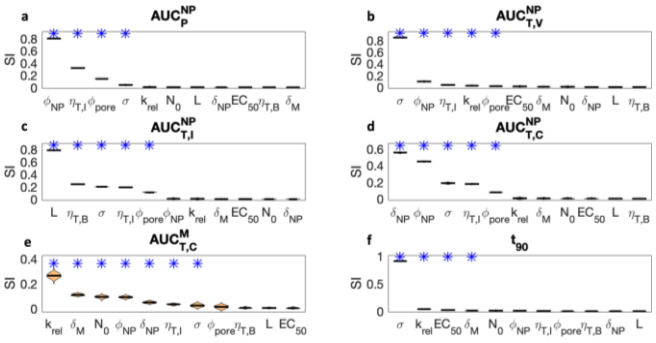

Figure 3. Global sensitivity analysis of model parameters for their effect on **a**) AUC_P^{NP}, **b**) $AUC_{T,V}^{NP}$, **c**) $AUC_{T,I}^{NP}$, **d**) $AUC_{T,C}^{NP}$, **e**) $AUC_{T,C}^{M}$, and **f**) t_{90}. Violin plots show distribution of sensitivity index (SI) (or regression coefficients of MLRA) for each parameter. Blue asterisk indicates parameters that play a significant role in governing the corresponding model output, as identified through MLRA ($p < 0.05$). Note: parameters are arranged in decreasing order of sensitivity from left to right.

median value (0.7 %ID) of NP accumulation in the tumor following a single injection [32].

The NPs accumulated in the cytosol release miRNA into the cytosol, such that as shown in Fig. 3e, miRNA release rate (k_{rel}) is the most significant factor, followed by degradation rate of miRNA (δ_M), in governing miRNA bioavailability in tumor cytosol ($\mathrm{AUC}_{T,C}^{\mathrm{M}}$). The reference parameter values of the hypothetical miRNA used in the study allow attainment of miRNA concentration in the cytosol greater than the reference EC_{50} value required for therapeutic efficacy, throughout the duration of treatment (Fig. 2e). As a result, as shown in Fig. 2f, following weekly injections of miRNA-loaded NPs, the tumor shows growth inhibition, resulting in a smaller size during the treatment timeframe in comparison to the control tumor. As observed, the treated tumor takes ~16 days longer to reach 90% carrying capacity (t_{90} = 5.35 wks), with respect to the no-treatment scenario (t_{90} = 3 wks). Note that t_{90} is only being used for the purpose of quantitative comparison and has no clinical relevance. However, post treatment termination, as the miRNA concentration falls below the effective threshold the treated tumor manages to reach the carrying capacity, equaling the untreated tumor in size. This can be attributed to the lack of a death mechanism in the logistic tumor growth model (Eq. 7). For simplicity, the model only contains a single mechanism of action via which the miRNA exhibits its effect, i.e., miRNA concentration-dependent suppression of tumor growth rate constant σ, which is the most significant factor in affecting tumor growth (Fig. 3f). However, to allow the possibility of miRNA-induced or co-administered chemotherapeutic-induced death, future updates to the pharmacodynamic component of the model will be necessary.

IV. Conclusion

Using a simplified, multicompartment mechanistic model, we studied the pharmacokinetic and pharmacodynamic aspects of NP-mediated miRNA therapy for tumor inhibition, and also investigated the effects of simultaneous parameter perturbations (through GSA) on key model outputs, including the bioavailability of NPs in various compartments, the bioavailability of miRNAs in tumor cytosol, and the resulting therapeutic outcome of miRNA-induced tumor growth inhibition. In addition to the importance of NP size, through the analysis we were also able to identify the importance of miRNA release rate from NPs and degradability of NPs in governing cytosolic accumulation of miRNAs, which directly impact tumor growth based on the EC_{50} of a given miRNA. These tunable NP properties thus provide opportunities to optimize the drug delivery system for enhancing the efficacy of miRNA therapy. This model represents a first step towards a more complete mechanistic model that can account for additional NP characteristics (e.g., targeting to improve endocytosis) and also include specific molecular signaling pathways in the cytosolic compartment to better represent the mechanisms of action of miRNAs.

References

[1] G. A. Calin *et al.*, *Proceedings of the National Academy of Sciences,* vol. 99, no. 24, pp. 15524-15529, 2002.
[2] L. He *et al.*, *Nature,* vol. 435, no. 7043, pp. 828-33, Jun 9, 2005.
[3] S. W. L. Lee *et al.*, *Journal of Controlled Release,* vol. 313, pp. 80-95, 2019.
[4] S. Goel *et al.*, *Science Advances,* vol. 6, no. 26, pp. eaba4498, 2020.
[5] Z. Wang *et al.*, *PLoS Comput Biol,* vol. 12, no. 6, pp. e1004969, Jun, 2016.
[6] V. Cristini *et al.*, *An Introduction to Physical Oncology: How Mechanistic Mathematical Modeling Can Improve Cancer Therapy Outcomes*: CRC Press, 2017.
[7] P. Dogra *et al.*, *Wiley Interdiscip Rev Nanomed Nanobiotechnol,* vol. 12, no. 5, pp. e1628, Sep, 2020.
[8] T. A. Brocato *et al.*, *Sci Rep,* vol. 8, no. 1, pp. 7538, May 24, 2018.
[9] P. Dogra *et al.*, *Nature Communications,* vol. 9, no. 1, pp. 4551, 2018.
[10] H. S. Choi *et al.*, *Nature biotechnology,* vol. 25, no. 10, pp. 1165, 2007.
[11] N. Hoshyar *et al.*, *Nanomedicine,* vol. 11, no. 6, pp. 673-692, 2016.
[12] S.-G. Kim, and J. J. Ackerman, *Cancer research,* vol. 48, no. 12, pp. 3449-3453, 1988.
[13] P. Dogra *et al.*, *Computational and Structural Biotechnology Journal,* vol. 18, pp. 518-531, 2020.
[14] R. K. Jain, *Cancer research,* vol. 48, no. 10, pp. 2641-2658, 1988.
[15] P. M. O'Connor *et al.*, *Cancer research,* vol. 57, no. 19, pp. 4285-4300, 1997.
[16] H. Hashizume *et al.*, *The American journal of pathology,* vol. 156, no. 4, pp. 1363-1380, 2000.
[17] M. Konerding *et al.*, *British journal of cancer,* vol. 80, no. 5, pp. 724-732, 1999.
[18] C.-T. Chen *et al.*, *Biorheology,* vol. 35, no. 2, pp. 103-118, 1998.
[19] X. Paez-Colasante *et al.*, *Frontiers in Cellular Neuroscience,* vol. 14, pp. 117, 2020.
[20] M. J. Marzi *et al.*, *Genome research,* vol. 26, no. 4, pp. 554-565, 2016.
[21] P. Dogra *et al.*, *Biomedical Microdevices,* vol. 21, no. 2, pp. 1-23, 2019.
[22] M. Mikubo *et al.*, *Journal of Thoracic Oncology,* vol. 15, no. 1, pp. 130-137, 2020.
[23] W.-W. Sung *et al.*, *BMC cancer,* vol. 14, no. 1, pp. 1-7, 2014.
[24] A. Gorur *et al.*, *Molecular Therapy-Nucleic Acids*, 2021.
[25] P. Dogra *et al.*, *ACS Pharmacol Transl Sci,* vol. 4, no. 1, pp. 248-265, Feb 12, 2021.
[26] Z. Wang *et al.*, *IET systems biology,* vol. 8, no. 5, pp. 191-197, 2014.
[27] Z. Wang *et al.*, *Front Physiol,* vol. 2, pp. 35, 2011.
[28] Z. Wang *et al.*, *Bioinformatics,* vol. 25, no. 18, pp. 2389-96, Sep 15, 2009.
[29] I. AAT Bioquest. "Quest Calculate™ RNA Molecular Weight Calculator.," 2/23/2021, 2021; https://www.aatbio.com/tools/calculate-RNA-molecular-weight-mw.
[30] H. P. Erickson, *Biological procedures online,* vol. 11, no. 1, pp. 32-51, 2009.
[31] S. Torquato *et al.*, *Physical review letters,* vol. 84, no. 10, pp. 2064, 2000.
[32] S. Wilhelm *et al.*, *Nature reviews materials,* vol. 1, no. 5, pp. 1-12, 2016.